AMERICAN SOCIETY FOR MICROBIOLOGY | Applied and Environmental Microbiology

Respiratory Kinetics of Marine Bacteria Exposed to Decreasing Oxygen Concentrations

Xianzhe Gong, Emilio Garcia-Robledo, Andreas Schramm, Niels Peter Revsbech

Section of Microbiology, Department of Bioscience, Aarhus University, Aarhus, Denmark

During aerobic respiration, microorganisms consume oxygen (O_2) through the use of different types of terminal oxidases which have a wide range of affinities for O_2. The K_m values for O_2 of these enzymes have been determined to be in the range of 3 to 200 nmol liter^{-1}. In this study, we examined the time course of development of aerobic respiratory kinetics of four marine bacterial species (*Dinoroseobacter shibae*, *Roseobacter denitrificans*, *Idiomarina loihiensis*, and *Marinobacter daepoensis*) during exposure to decreasing O_2 concentrations. The genomes of all four species have genes for both high-affinity and low-affinity terminal oxidases. The respiration rate of the bacteria was measured by the use of extremely sensitive optical trace O_2 sensors (range, 1 to 1,000 nmol liter^{-1}). Three of the four isolates exhibited apparent K_m values of 30 to 60 nmol liter^{-1} when exposed to submicromolar O_2 concentrations, but a decrease to values below 10 nmol liter^{-1} was observed when the respiration rate per cell was lowered and the cell size was decreased due to starvation. The fourth isolate did not reach a low respiration rate per cell during starvation and exhibited apparent K_m values of about 20 nmol liter^{-1} throughout the experiment. The results clearly demonstrate not only that enzyme kinetics may limit O_2 uptake but also that even individual cells may be diffusion limited and that this diffusion limitation is the most pronounced at high respiration rates. A decrease in cell size by starvation, due to limiting organic carbon, and thereby more efficient diffusion uptake may also contribute to lower apparent K_m values.

Oxygen (O_2), the second most abundant gas in the atmosphere on Earth, plays a critical role in nature, including aquatic environments. As the most favorable electron acceptor, O_2 drives the degradation of organic matter and influences the cycling of other elements (e.g., nitrogen, sulfur, phosphorus) (1). For decades, aerobic respiration has been studied by different methods in various environments (2–4). Due to the limit of detection by traditional methods (Winkler methods and methods that use electrochemical sensors and optodes), the measurement of respiratory activity in low-O_2 environments, such as oceanic oxygen-minimum zones (OMZs), is rare (5), and even in fully oxygenated waters, the direct measurement of oxygen dynamics is difficult and the more indirect method of measurement of formazan formation has therefore been applied (6). The lack of detailed data on aerobic respiration in low-O_2 environments restricts the understanding of carbon budgets (7) and the prediction of the development of O_2 within such environments (8). Recently, STOX oxygen sensors have been applied to quantify O_2 respiration rates in OMZs (9), and by this technique, it was possible to measure rates down to about 1 nmol^{-1} liter^{-1} h^{-1}, which is a level of resolution that is a factor of 10 higher than that obtained by traditional methods (10). Half-saturation constants (apparent K_m values) for microbial communities were estimated from the data obtained with STOX oxygen sensors, but highly variable values ranging from 30 to 200 nmol liter^{-1} were obtained. Another study indicated high half-saturation O_2 concentrations of several micromolar, supposedly caused by diffusion limitation around and within aggregates (11).

The final step of aerobic respiration is conducted by a terminal cytochrome oxidase, a membrane-associated protein which transfers electrons to O_2 (12). Two main families of terminal oxidases have been classified on the basis of structural and functional differences (13–16): the heme-copper oxidases (HCOs) and the cytochrome *bd*-type oxidases. Furthermore, three classes have been identified within HCOs according to the combination of different heme subunits (classes A, B, and C). The kinetic parameters maximum respiration rate (V_{max}) and K_m can be used to describe respiratory activity as a function of the O_2 concentration, although it should be kept in mind that the Michaelis-Menten equation strictly applies only to the kinetics of single enzymes. According to the affinity of O_2, these terminal oxidases can be classified as high-affinity terminal oxidases (with K_m values of about 3 to 8 nmol liter^{-1}) (17) and low-affinity terminal oxidases (with K_m values of about 200 nmol liter^{-1}) (18). Respiration rates in aquatic environments have been estimated by different methods, and the kinetics have been estimated using several models. Different equations have been proposed to estimate V_{max} and K_m values, such as fitting of the data directly to the Michaelis-Menten equation by computer-aided iterative regression (19); the method of Dixon and Webb, as described by Kita et al. (20); and the method described by Appleby and Bergersen (21). Tiano et al. (22) reported that a modified Jassby and Platt equation results in better fits to the measured decrease in the O_2 concentration than the Michaelis-Menten model under low O_2 concentrations.

The microbial aerobic respiration rate is affected by different factors, such as growth phase, nutrient availability, and the O_2 concentration. On the basis of genomic data analysis, some bacteria have both high- and low-affinity terminal oxidase genes, and the high-affinity terminal oxidases may enable these bacteria to

Received 10 November 2015 **Accepted** 12 December 2015

Accepted manuscript posted online 18 December 2015

Citation Gong X, Garcia-Robledo E, Schramm A, Revsbech NP. 2016. Respiratory kinetics of marine bacteria exposed to decreasing oxygen concentrations. Appl Environ Microbiol 82:1412–1422. doi:10.1128/AEM.03669-15.

Editor: S.-J. Liu, Chinese Academy of Sciences

Address correspondence to Niels Peter Revsbech, revsbech@bios.au.dk.

maintain high levels of respiratory activity down to low-nanomolar levels of O_2 (17, 18). It has, however, been difficult to measure the O_2 concentration when it is present at such low concentrations, and the few investigations of O_2 at the nanomolar level that have been performed have been done by spectroscopy of oxygenated/deoxygenated leghemoglobins or myoglobins, yielding information about changes in O_2 levels only over a very limited range of O_2 concentrations without the possibility of investigating the change in kinetics after exposure to conditions with low O_2 concentrations (23). Little attention has thus been paid to the kinetics of microbial respiration in marine environments, where low-oxygen conditions prevail in many areas, such as in OMZs. The respiratory activities in north and south eastern tropical Pacific OMZs were found to change with depth, and even the same water sample showed changes in activity under different initial conditions of O_2 incubation, which indicates a fast adaptation of the microbial community to changing environmental conditions (9).

In this study, we investigated the respiratory kinetics of pure cultures of marine bacteria to get insight into the basic mechanisms of respiration under low-O_2 conditions. The use of pure cultures of marine bacteria provides information on respiration under low-O_2 conditions better than that which we can obtain by analyzing heterogeneous marine communities. The change in bacterial respiratory activity was thus examined by incubation of four pure cultures of marine bacteria known to have both high- and low-affinity terminal oxidases in the presence of low O_2 concentrations. The incubations were performed both with an ample supply of electron donors and under starvation conditions. The respiration rates were determined in all-glass setups to avoid contamination with O_2, and the concentrations of O_2 were determined with novel highly sensitive optodes that can resolve nanomolar concentrations over the range of 1 to 1,000 nmol liter^{-1} (24). The setup enabled us to take samples over the period of incubation to evaluate cell numbers by flow cytometry and cell size by fluorescence microscopy.

MATERIALS AND METHODS

Bacterial culture preparation. Four strains of bacteria (*Dinoroseobacter shibae* DSM-16493, *Roseobacter denitrificans* DSM-7001, *Idiomarina loihiensis* DSM-15497, and *Marinobacter daepoensis* DSM-16072) were purchased from the Leibniz Institute, DSMZ, Germany. Bacteria were grown at 25°C on autoclaved marine broth medium containing 5.00 g peptone (BD), 1.00 g yeast extract (Difco), 0.10 g $FeC_6H_5O_7$, 12.60 g $MgCl_2{\cdot}6H_2O$, 3.24 g Na_2SO_4, 19.45 g NaCl, 2.38 g $CaCl_2{\cdot}2H_2O$, 0.55 g KCl, 0.16 g $NaHCO_3$, and 0.01 g $Na_2HPO_4{\cdot}2H_2O$ per liter. Cultures were incubated on a rotary shaker (180 rpm) to ensure fully oxic conditions and to obtain cell suspensions in exponential growth phase.

Setup and incubation. The Lumos optode optoelectronics device (24) was held by a polyvinyl chloride holder, which was glued on the outside of the bottle. The photodetector was aligned with the preglued glass dot, which was coated with a thin layer of the fluorophore [palladium(II) 5,10,15,20-tetrakis-(2,3,4,5,6-pentafluorphenyl)-porphyrin] in Hyflon AD 60 perfluoropolymer (25) (coated glass dots are referred to here as optode dots). The combination of the specific fluorophore and Hyflon AD 60 results in a highly sensitive optode that can measure concentrations ranging from 1 to 1,000 nmol liter^{-1}. The Lumos device was connected to a computer and was controlled by FireSting Logger software (Pyroscience). Data were recorded every 15 s during the incubations.

Artificial seawater was utilized for bacterial incubation and was prepared as described previously (26). It consisted of 24.99 g NaCl, 4.16 g Na_2SO_4, 0.79 g KCl, 0.18 g $NaHCO_3$, and individually autoclaved 11.13 g $MgCl_2{\cdot}6H_2O$ and 1.58 g $CaCl_2{\cdot}2H_2O$ per liter. The pH was adjusted to 7.5 after the different components of the seawater were mixed.

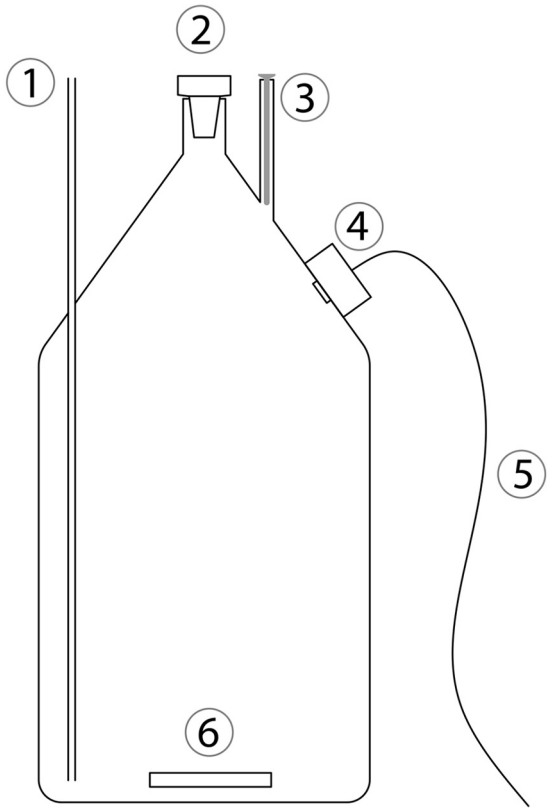

FIG 1 Schematic drawing of the bottle used for incubation. 1, pressure compensation tube; 2, ground-glass stopper; 3, glass tube with an internal diameter of 8.1 mm for insertion of an 8-mm-diameter STOX sensor (for these experiments, a STOX dummy was inserted); 4, optode with optoelectronics; 5, wire for connection to a personal computer for data collection; 6, glass-coated magnet.

The details of the setup (Fig. 1) and the procedure conducted have been described by Tiano et al. (22). Briefly, seawater was bubbled with N_2 for 1 h to remove the dissolved O_2 without dramatically changing the pH. Modified bottles with preglued optode dots inside and a glass-coated magnet in the bottom were filled by use of a Tygon and glass tube siphon connected to the reservoir. The reservoir and the gas phase of the bottles were continuously flushed with N_2. All bottles, glass-coated magnets, and tubes had previously been cleaned with 0.1 M HCl and subsequently washed with autoclaved water to minimize bacterial contamination. The bottles (volume, 1,160 ml) had a thin (internal diameter, 0.25 cm) and long (length, 25 cm) glass tube, hereafter named the pressure compensation tube, penetrating the glass wall at the periphery of the bottle to allow a change in volume caused by temperature variations and to enable addition and removal of liquid during the incubations.

During the incubations, the bottles were kept in a water bath kept at a constant temperature of 25°C. Before injection of the bacteria, the bottles with seawater were kept in the water bath for 30 min to reach temperature equilibrium. The incubations lasted for 30 to 40 h.

In order to estimate the growth phase of the bacteria in the inoculum, the optical density at 600 nm was measured with a spectrophotometer (Pharmacia Biotech). The culture was adjusted to the proper concentration with marine broth medium, and a small amount of culture was injected into the incubation bottles to ensure a suitable respiration rate. Data for dilutions and injection volumes are shown in Table 1. One milliliter of air-saturated water was repeatedly injected into the bottles (cor-

TABLE 1 OD_{600}, dilution before injection, and volume of injection into the reactors for *M. daepoensis*, *I. loihiensis*, *D. shibae*, and *R. denitrificans*

Species	Limitation[a]	OD_{600}[b]	Dilution (fold)	Injection vol (ml)
M. daepoensis	No	0.090	6	1
	Yes	0.566	5	0.4
I. loihiensis	No	0.137	9	1
	Yes	1.104	5	0.4
R. denitrificans	No	1.049	7	0.4
	Yes	1.244	2	0.4
D. shibae	No	0.235	5	1
	Yes	0.397	1.2	0.4

[a] One of the incubations for each culture was designed to cause severe electron donor limitation and is indicated by "Yes."
[b] Data represent the mean values from three experiments.

responding to an increase in the O_2 concentration of approximately 300 nmol liter^{-1}) when the optode reading indicated anoxia. A long syringe needle that could penetrate the whole pressure compensation tube was used for the injections (and also for the removal of samples). The injection of air-saturated water also served for calibration of the sensor. Samples of 1 ml liquid for microscopic and flow cytometry analysis were taken through the pressure compensation tube every 5 h during the incubation, while 1 ml of oxic water was simultaneously injected. The water sample was fixed with 1% glutaraldehyde (Sigma) at room temperature for 10 min, shock frozen in liquid nitrogen, and stored in a −80°C freezer until further analysis.

Determination of cell numbers by flow cytometry. Bacterial numbers were determined using a NovoCyte flow cytometer (ACEA Biosciences) equipped with a 488-nm laser and a 530-nm filter. Subsamples (100 μl) were stained with 1 μl of an 8×-diluted solution of SYTO 13 (Molecular Probes) for 15 min prior to the counting of the number of cells. The abundance of bacteria was determined by counting the bacteria contained in a fixed sample volume of 25 μl. The number of bacteria in a region in a scatterplot of the SYTO 13 fluorescence signal versus the side scatter that was used for counting was determined by comparison with the number of bacteria in a sample that was not stained.

Measurement of cell size by fluorescence microscopy. One hundred microliters of fixed sample was filtered onto 0.2-μm-pore-size polycarbonate filters (Maine Manufacturing LLC). The dried samples were stained with 1 drop of prepared SYBR green (1 μl of SYBR green I nucleic acid gel stain [Thermo Fisher Scientific] mixed with 800 μl of glycerol–phosphate-buffered saline [AF1; CitiFluor Ltd.] and 200 μl of Vectashield mounting medium [Vector Laboratories]). Cell sizes were measured using an Axiovert 200M epifluorescence microscope with standard SYBR green and fluorescein filter sets (Zeiss). At least 400 cells per sample were measured. It is difficult to measure an accurate size by fluorescence, but it is possible to observe relative changes in size.

Data analysis and modeling of kinetic parameters and population size. Two kinetic parameters, the respiration rate of the population and the half-saturation constant (apparent K_m), were estimated by use of a modified Jassby and Platt equation as described by Tiano et al. (22). The cell numbers between the two measurement time points were estimated by linear interpolation. The respiration rate per cell was calculated by dividing the respiration rate of the population by the cell numbers.

Statistical analysis and graphing. To determine if there was a significant difference in the apparent K_m values determined during the incubation, the apparent K_m values obtained over time were tested by the Tukey test in a one-way repeated-measures analysis of variance (ANOVA). If the normality test (Shapiro-Wilk) or equal variance test failed, the data were transformed by use of a $\log(x + 1)$ transformation. The Friedman test was used if the transformed data still failed the normality test or the equal variance test. Differences in doubling times and cell sizes during the incubations were tested by *t* test. The significance value was set at 0.05 for multiple comparisons in *post hoc* tests. All the data were plotted by the SigmaPlot (version 12.0) program to construct the figures.

RESULTS

As the setup applied in this study allowed us to measure O_2 concentrations over time, it was possible to monitor and analyze the respiratory activity with a high degree of temporal resolution (Fig. 2). The initial O_2 concentration during the initial incubation was about 200 nmol liter^{-1}. Subsequent injections of aerated water increased the O_2 concentration to about 300 nmol liter^{-1} right after the injections (Fig. 2).

The estimated apparent K_m values and respiration rates of the population during the incubations are plotted in Fig. 3 and Fig. 4. The respiration rate of the population during the first type of incubation progressively increased during the whole period of measurement, and therefore, that type of incubation could be considered to have taken place under non-energy-limited (i.e., non-electron-donor-limited) conditions (Fig. 3). The initial respiration rates of the *M. daepoensis* and *I. loihiensis* populations (46 ± 15 and 29 ± 8 nmol O_2 liter^{-1} h^{-1}, respectively) were lower than those of the *R. denitrificans* and *D. shibae* populations (177 ± 28 and 128 ± 23 nmol O_2 liter^{-1} h^{-1}, respectively). However, the final respiration rates of the populations during the incubation were 1,450 ± 203, 1,724 ± 108, 609 ± 22, and 537 ± 52 nmol O_2 liter^{-1} h^{-1} for *M. daepoensis*, *I. loihiensis*, *R. denitrificans*, and *D. shibae*, respectively. These increased respira-

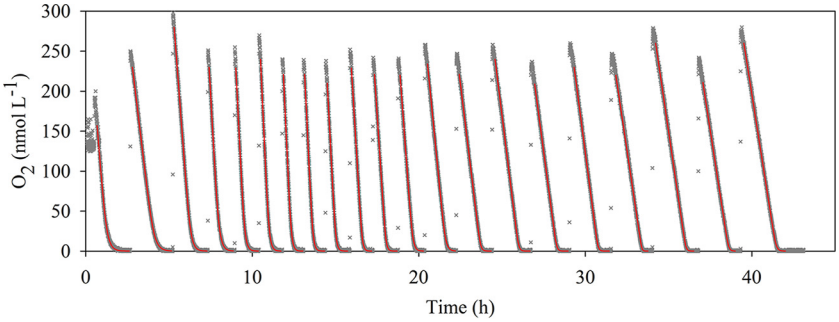

FIG 2 Time course of the oxygen concentration during 42 h of incubation of *R. denitrificans* with artificial seawater under energy-limited conditions. During the incubation, 1 ml of air-saturated water was injected into the bottle through the pressure compensation tube when oxygen was completely consumed. Gray crosses, the data points measured every 15 s (most are hidden by the red curves); red curves, the modeled curves used for extraction of the kinetic parameters.

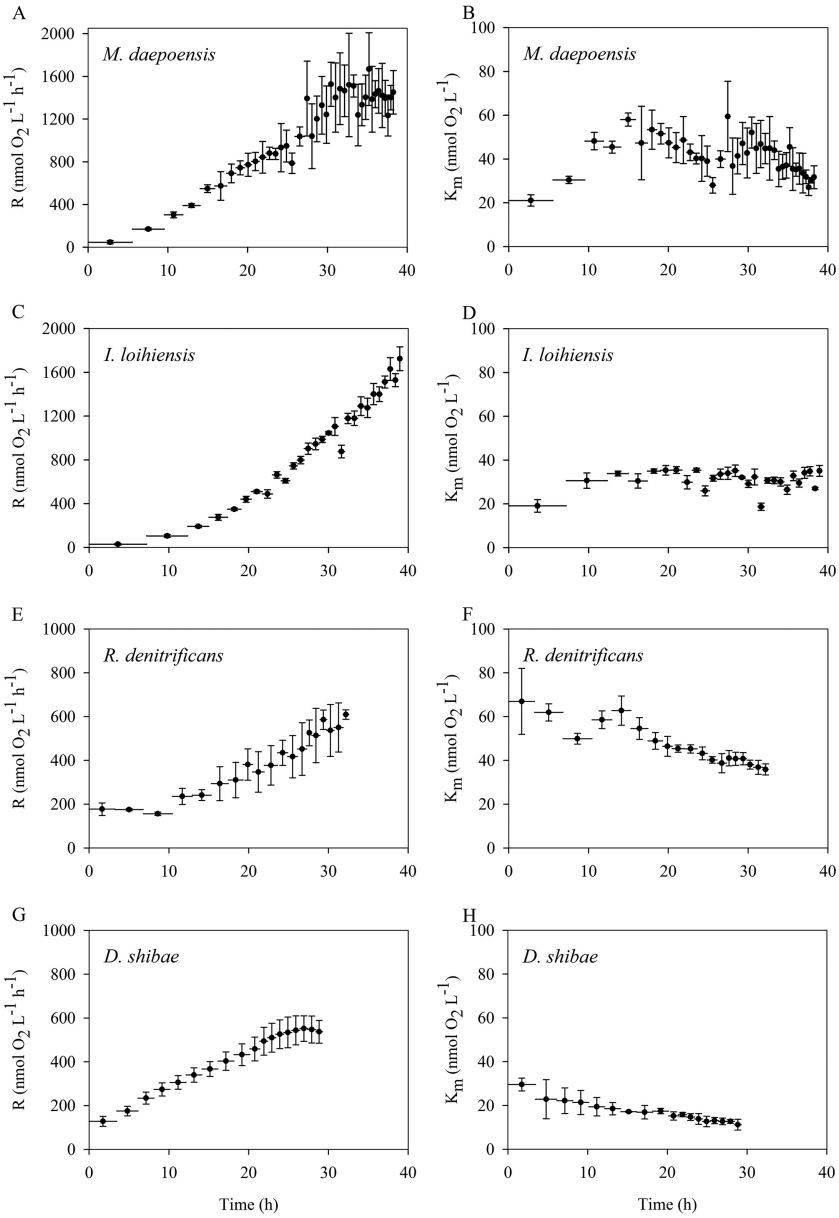

FIG 3 Time course of the respiration rates (R) of the population (A, C, E, and G) and apparent K_m values (B, D, F, and H) for four species, *M. daepoensis* (A and B), *I. loihiensis* (C and D), *R. denitrificans* (E and F), and *D. shibae* (G and H), during incubation under non-energy-limited conditions. Values are means ± SDs ($n = 3$ or 4). Horizontal bars represent time periods. Note the differences in the *y*-axis scales in the left panels (A, C, E, and G).

tion rates for the populations indicate growth of the bacteria, and *M. daepoensis* and *I. loihiensis* especially exhibited high growth rates. The apparent K_m value for *I. loihiensis* was about 30 nmol liter^{-1}. The apparent K_m value decreased from 66 ± 15 to 35 ± 2 nmol liter^{-1} and from 29 ± 3 to 11 ± 2 nmol liter^{-1} for *R. denitrificans*, and *D. shibae*, respectively. The apparent K_m value for *M. daepoensis* increased from about 27 ± 3 to 45 ± 3 mol liter^{-1} within the first 10 h and was subsequently stable for the next 20 h and then decreased to about 30 ± 1 nmol liter^{-1} after a total of 38 h of incubation. It is evident that after approximately 2 to 3 h the first data points for K_m values deviated somewhat from the other data points, indicating adaptation to new environmental conditions.

The second type of incubation was with injections of larger amounts of bacteria and smaller amounts of medium. With increases in the incubation period and the growth of the population, the respiration rate of the population increased for a period of time and then decreased dramatically (Fig. 4). This incubation was thus considered to have taken place under energy-limited conditions. The maximum values of the respiration rates of the populations during the incubation were 1,071 ± 85, 1,903 ± 75, 438 ± 9, and 1,243 ± 92 O_2 nmol liter^{-1} h^{-1} for *M. daepoensis*, *I. loihiensis*, *R. denitrificans*, and *D. shibae*, respectively. The initial apparent K_m values ranged from 35 ± 8 to 55 ± 16 nmol liter^{-1}, and the K_m values for all four species became stable when the respiration rates of the population reached the maximum. The apparent K_m values

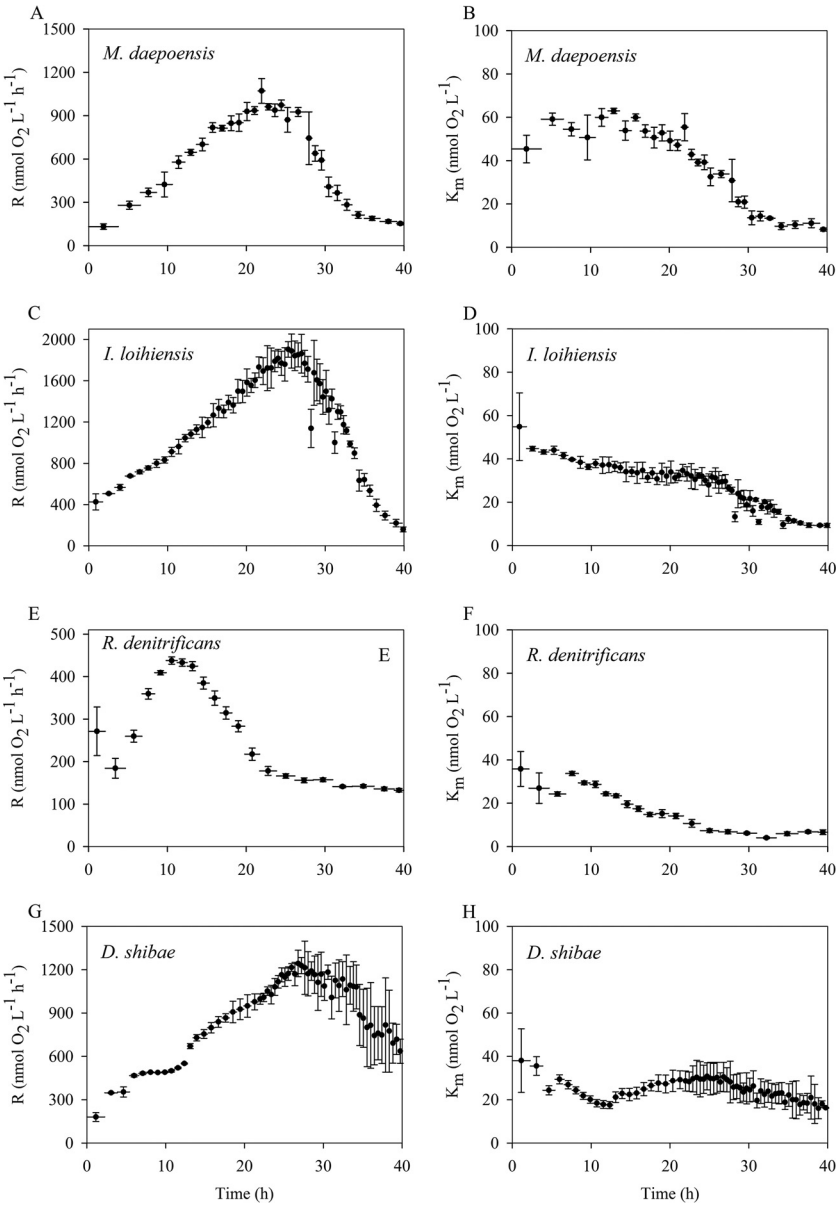

FIG 4 Time course of the respiration rates (R) of the population (A, C, E, and G) and apparent K_m values (B, D, F, and H) for four species, *M. daepoensis* (A and B), *I. loihiensis* (C and D), *R. denitrificans* (E and F), and *D. shibae* (G and H), during incubation over a period characterized by energy-limited conditions. Values are means ± SDs (n = 3 to 4). The horizontal bars represent time periods. Note the differences in the y-axis scales in the left panels (A, C, E, and G).

were thus 49 ± 4 nmol liter^{-1} at 20 h for *M. daepoensis*, 32 ± 4 nmol liter^{-1} at 24 h for *I. loihiensis*, 29 ± 1 nmol liter^{-1} at 10 h for *R. denitrificans*, and 29 ± 7 nmol liter^{-1} at 25 h for *D. shibae*. The apparent K_m values subsequently decreased and the respiration rates of the populations decreased during starvation, and the K_m values gradually reached final low levels that were slightly different for the different cultures. The final stable K_m values were 8 ± 1, 9 ± 1, 7 ± 1, and 16 ± 1 nmol liter^{-1} for *M. daepoensis*, *I. loihiensis*, *R. denitrificans*, and *D. shibae*, respectively. The *D. shibae* culture did not, however, exhibit the same large decrease in apparent K_m value that the other cultures did, probably because the incubation time was insufficient for it to reach low rates of respiration per cell.

The population sizes and respiration rate per cell of *M. daepoensis* and *I. loihiensis* were tracked during incubation under non-energy-limited conditions (Fig. 5) and under energy-limited conditions (Fig. 6). The population sizes increased for all four incubations, and the cultures grew in terms of cell number (but not total biovolume; see below) only slightly faster under non-energy-limited conditions than under energy-limited conditions. During the incubation under non-energy-limited condition (Fig. 5), the respiration rate of *M. daepoensis* increased from 0.80 ± 0.24 to 2.61 ± 0.21 fmol O_2 cell^{-1} h^{-1} at about 15 h and then decreased to 1.00 ± 0.09 fmol O_2 cell^{-1} h^{-1} at the end of the incubation; the respiration rate of *I. loihiensis* increased from 0.26 ± 0.07 to 0.80 ± 0.08 fmol O_2 cell^{-1} h^{-1} at about 23 h, and the respiration rate stayed at this level during the rest of the incubation. The low respiration rates obtained from the first determi-

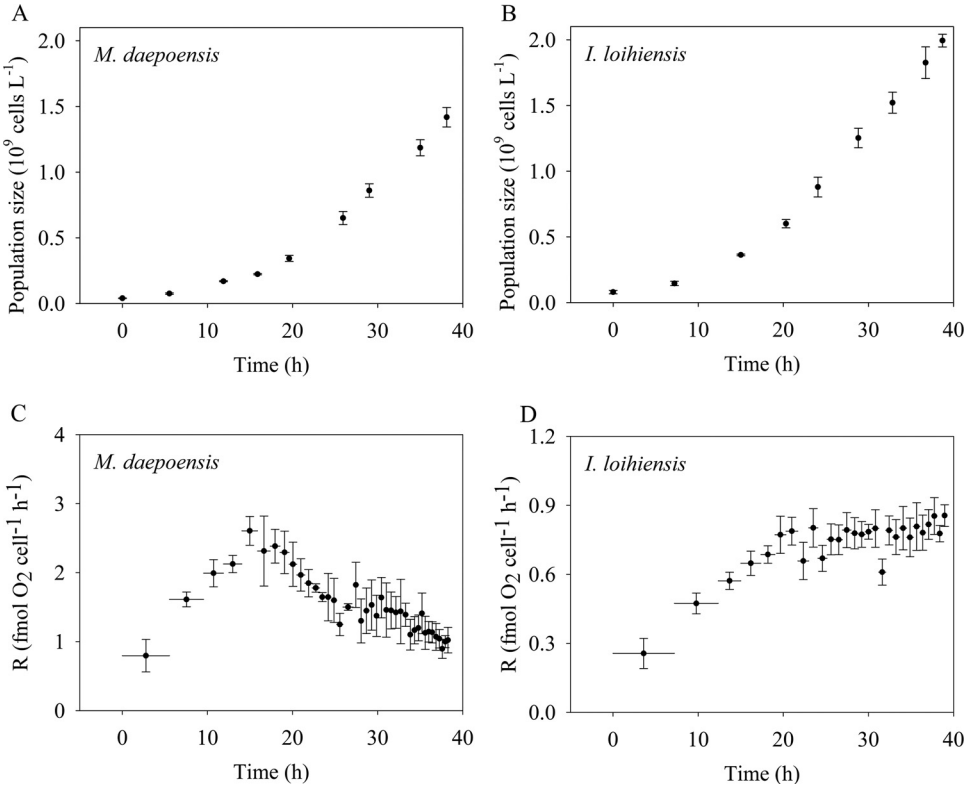

FIG 5 Time courses of population size (A and B) and the respiration rate per cell (*R*) (C and D) of *M. daepoensis* and *I. loihiensis* during incubation under non-energy-limited conditions. Values are means ± SDs ($n = 3$ to 4). The horizontal bars (C and D) represent time periods. Note the differences in the *y*-axis scales in the bottom panels (C and D).

nations indicated a lag phase before maximum growth under the new culture conditions. During the incubation under energy-limited condition (Fig. 6), the respiration rate of *M. daepoensis* increased from 1.54 ± 0.51 to 2.44 ± 0.35 fmol O_2 $cell^{-1}$ h^{-1} at about 11 h and then decreased to a very low rate (0.12 fmol O_2 $cell^{-1}$ h^{-1}) at the end of the incubation; the respiration rate of *I. loihiensis* decreased from 0.85 ± 0.16 to 0.70 ± 0.02 fmol O_2 $cell^{-1}$ h^{-1} at about 7 h and then decreased to a very low rate (0.03 ± 0.004 fmol O_2 $cell^{-1}$ h^{-1}) at the end of the incubation.

The cell sizes of *M. daepoensis* during the incubation under energy-limited condition were measured under a fluorescence microscope with SYBR green staining. The lengths of the cells (Fig. 7) decreased significantly ($P < 0.05$, *t* test), due to starvation, from 1.80 ± 0.43 μm at the beginning of the incubation to 1.72 ± 0.44 μm at 12.6 h during the incubation and further decreased to 1.16 ± 0.27 μm at the end of the incubation. Although the cell number increased during incubation under energy-limited conditions, this did not correspond to a proportional increase in the total biovolume.

DISCUSSION

The study of O_2 kinetics at low O_2 concentrations requires sensors with high degrees of accuracy at low O_2 concentrations, an incubation vessel that does not leak O_2 into the system, and a homogeneous culture without aggregate formation. The setup applied in this experiment was tested in a previous study (22). The long pressure compensation tube is the only entry for O_2 exchange in this glass-sealed system. It was proven both by mathematical calculation and with experimental data (22) that the O_2 exchange between the incubation vessel and the environment is negligible. The glass-coated magnet in the bottle ensures homogeneity after injections of bacteria or O_2-saturated water. During this experiment, two bottles into which bacteria were not injected were used as controls in each run. The results from these noninoculated bottles also confirmed that there was no external O_2 contamination (data not shown).

During our incubations, the cells were exposed to multiple oxic/anoxic shifts. The effects of a change from anoxic to oxic conditions have been investigated in detail for *D. shibae*, and it was concluded that the energy charge of the cell was back to normal oxic values within less than a minute (27). We assume that the same also held true for the other three organisms and that our measurements of energy metabolism, expressed by the rates of O_2 consumption during about 10-min periods of oxic conditions, represent short-term steady-state values (not taking the O_2 concentration dependence into account). The prolonged exposure of cultures to anoxia may lead to significant physiological changes (28), and we thus avoided long anoxic periods.

On the basis of an analysis of genomics data, the genomes of all four investigated species have the genes for both high-affinity terminal oxidases and low-affinity terminal oxidases. Thus, they all have the potential to have low apparent K_m values by expressing the high-affinity terminal oxidases. During the incubation under non-energy-limited, low-oxygen conditions, the slight decrease in the apparent K_m values for *R. denitrificans* and *D. shibae* may indicate the expression of a high-affinity termi-

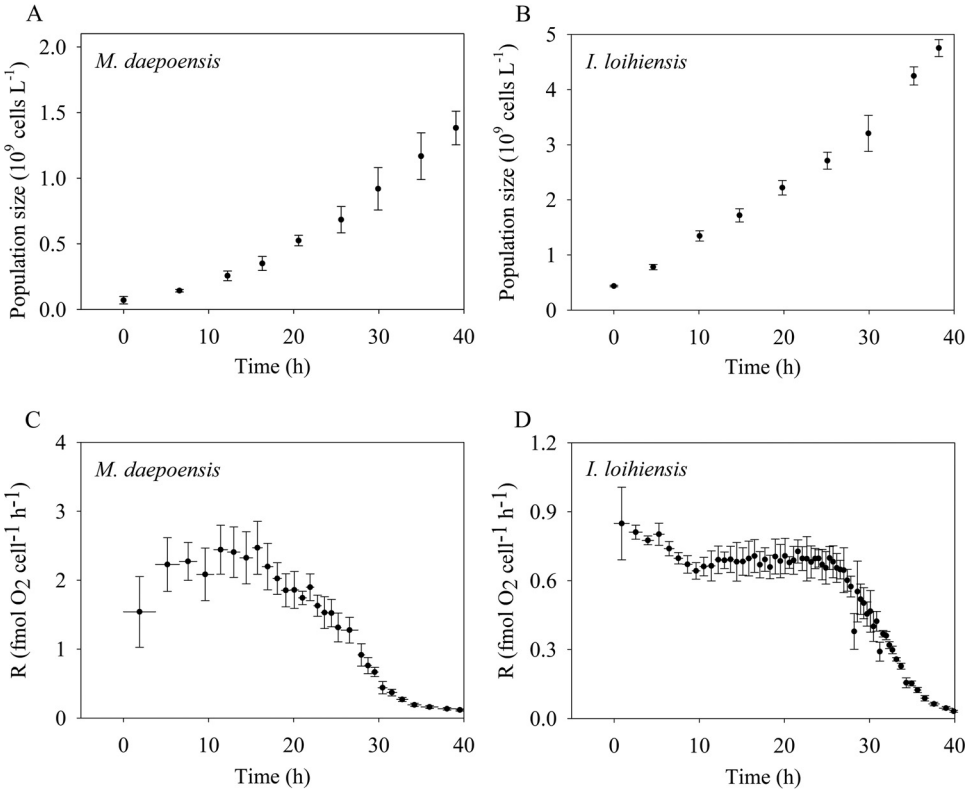

FIG 6 Time courses of population size (A and B) and the respiration rate per cell (*R*) (C and D) of *M. daepoensis* and *I. loihiensis* during incubation under energy-limited conditions. Values are means ± SDs ($n = 3$ to 4). The horizontal bars (C and D) represent time periods. Note the differences in the *y*-axis scales in the bottom panels (C and D).

nal oxidase. Considering that the K_m value of low-affinity terminal oxidases is about 200 nmol liter^{-1} (18) and that of high-affinity terminal oxidases is 3 to 8 nmol liter^{-1} (17), the estimated apparent K_m values for *M. daepoensis* (about 43 nmol liter^{-1}) and *I. loihiensis* (about 31 nmol liter^{-1}) demonstrate that large portions of the terminal oxidases were the high-affinity ones. A gene fusion study with *Escherichia coli* (29) showed that genes for high-affinity terminal oxidases are expressed under high-O_2 conditions, and even cultures incubated under high-O_2 conditions may thus exhibit relatively low apparent K_m values. *M. daepoensis* and *I. loihiensis* could have lowered their relatively high apparent K_m values during the incubation under non-energy-limited condition by decreasing their cell size, but cell size may be governed more by nutrient availability than by O_2 concentration. The only source of organic electron donors in our incubations was the organic matter remaining in the culture medium from the injection and internal storage, for example, as polyhydroxybutyric acid. Thus, the electron donors became limiting during the incubations with large amounts of bacteria and small amounts of medium. The population size continued to increase during the periods when the respiration rate of the populations decreased due to starvation. The respiration rate per cell thus decreased dramatically. Meanwhile, it was accompanied by decreasing apparent K_m values, suggesting that the apparent K_m value was correlated with the availability of an electron donor.

In the following, the integrated effect of O_2 gradients around the cell, the difference in cell size, and the difference in respiration rate on the observed apparent K_m value are illustrated by modeling. For the convenience of modeling, the cells were assumed to be spherical but to have the same volume as the actual rod-shaped cells. We modeled the following three parameters. (i) The maximum O_2 flux to a cell with zero concentration at the cell surface (J_{max}) is given by (28)

$$J_{max} = 4\pi r_c D C_\infty \quad (1)$$

where r_c is the radius of the cell; D is the diffusion coefficient in water, which has a value of 2.40×10^{-5} cm^2 s^{-1} at 25°C; and C_∞ is the surrounding bulk O_2concentration.

(ii) The theoretical maximum respiration rate without diffusion limitation (R_{max}) can be described by the Michaelis-Menten equation:

$$R_{max} = V_{max} \frac{C_\infty}{C_\infty + K_m} \quad (2)$$

where K_m is the enzyme half-saturation concentration and V_{max} is the maximum respiration rate per cell at nonlimiting high O_2 concentrations.

(iii) The real respiration rate per cell (R_c) when diffusion limitation is taken into account is given by

$$R_c = V_{max} \times \frac{C_0}{C_0 + K_m} \quad (3)$$

where C_0 is the O_2 concentration at the cell surface, where the terminal oxidase is located.

The flux of O_2 to the cell (J) is defined by (30)

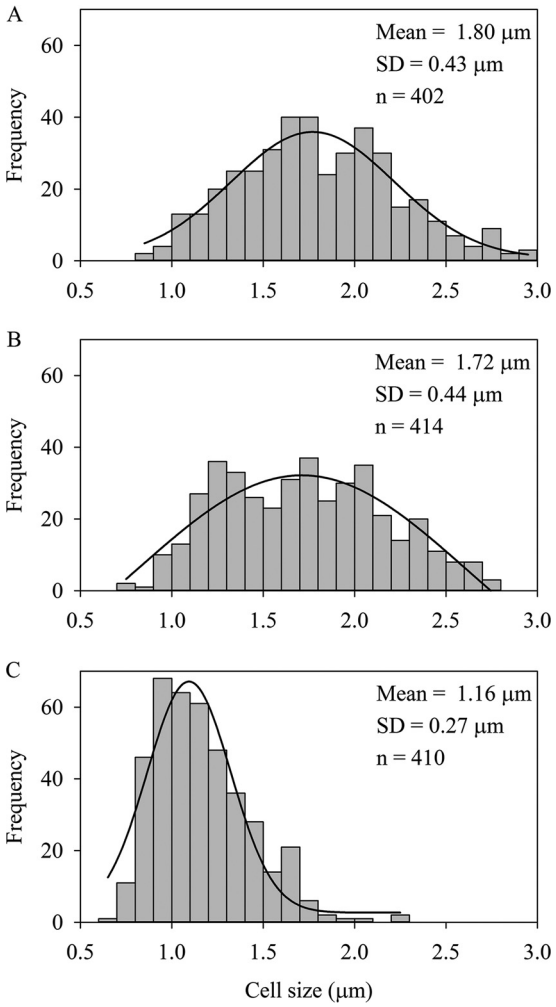

FIG 7 Cell size distribution of *M. daepoensis* at 0 h (A), 12.6 h (B), and 39.2 h (C) during incubation under energy-limited conditions.

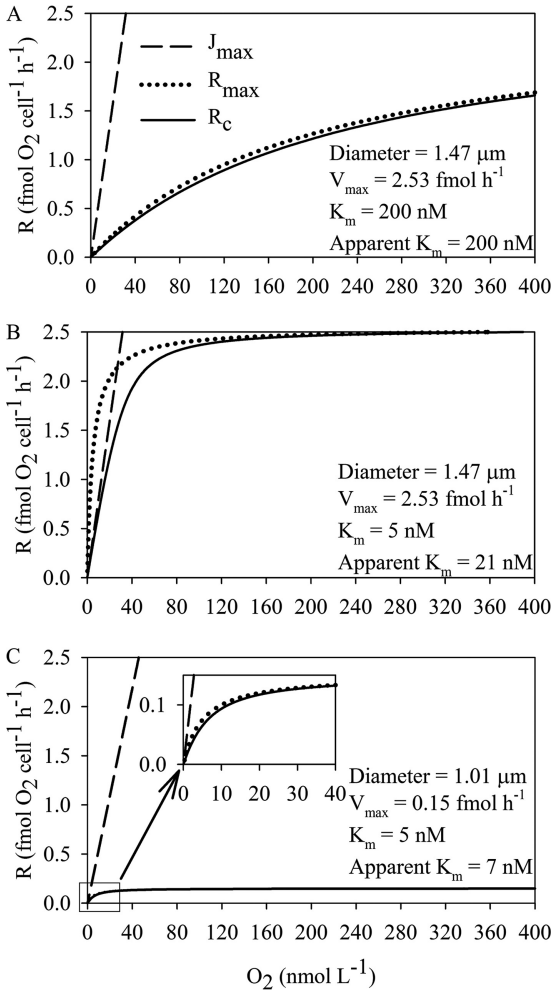

FIG 8 Modeled curves of O_2 consumption (R) of hypothetical spherical cells otherwise having characteristics similar to those of the *M. daepoensis* cells investigated under the following assumptions. (i) The cell consumes all oxygen diffusing to the cell so that the O_2 concentration at the cell surface is zero (J_{max}). (ii) The cell terminal oxidases exhibit Michaelis-Menten kinetics, but there is no diffusion limitation (R_{max}). (iii) The O_2 consumption by the cell is limited by both enzyme kinetics and diffusion to the cell (R_c). The modeling was performed under three scenarios: big cells (diameter, 1.47 µm) with a high respiration rate (2.53 fmol O_2 cell^{-1} h^{-1}) under nonlimiting O_2 concentrations (V_{max}) and only a low-affinity terminal oxidase (K_m value, 200 nmol liter^{-1}) (A), big cells with a high respiration rate and only a high-affinity terminal oxidase (K_m value, 5 nmol liter^{-1}) (B), and small cells (diameter, 1.01 µm) with a low respiration rate (0.20 fmol O_2 cell^{-1} h^{-1}) and only a high-affinity terminal oxidase (C).

$$J = 4\pi r_c D(C_\infty - C_0) \quad (4)$$

When the cell is in a steady state, the processes are balanced and the O_2 flux to the cell and the respiration rate per cell are equal:

$$R_c = J \quad (5)$$

Substitution from equations 3 and 4 gives

$$V_{max} \times \frac{C_0}{C_0 + K_m} = 4\pi r_c D(C_\infty - C_0) \quad (6)$$

C_0 can then be calculated with known values of V_{max}, K_m, r_c, and C_∞. Thus, R_c can be calculated in return as a function of C_∞.

In order to explain the model, we discuss here the data for *M. daepoensis* assuming two values for respiration under saturating O_2 concentrations (V_{max}), two different cell sizes, and two different K_m values. The large cell representative of the cell size under nonlimited conditions has an equivalent diameter of 1.47 µm, and the small cell representative of the cell size under conditions of starvation has an equivalent diameter of 1.01 µm. The diameters of cells of both sizes were recalculated from values in the literature (31) equating the diameters of cells with a rod shape to the diameters of spherical cells of the same volume. In the example, the large cell is assumed to be from the nonlimited condition with a high V_{max} (2.53 fmol O_2 cell^{-1} h^{-1}) and the small cell has a low V_{max} (0.15 fmol O_2 cell^{-1} h^{-1}). The actual respiration rate per cell by consideration of both diffusion limitation and Michaelis-Menten enzymatic kinetics (R_c), the maximum O_2 flux to the cell under the assumption that the O_2 concentration at the cell surface is 0 (J_{max}), and the theoretical maximum respiration rate per cell under the assumption that there is no diffusion limitation (R_{max}) were compared under three scenarios. (i) When the energy and O_2 supplies are sufficient, the cell size of *M. daepoensis* is assumed to be large, the respiration rate per cell is high, and only low-affinity terminal oxidases are expressed (K_m value, 200 nmol liter^{-1})

(Fig. 8A). In that case, the actual respiration rate is close to the theoretical maximum respiration rate, if no diffusion limitation at all O_2 concentrations is assumed, and the apparent K_m is identical to the enzyme K_m. Due to the high K_m value, both calculated respiration rates are much lower than J_{max}. (ii) In the second example, we consider large *M. daepoensis* cells having the same V_{max} of 2.53 fmol O_2 cell^{-1} h^{-1}, but now we assume that only high-affinity terminal oxidases are present (K_m value, 5 nmol liter^{-1}) (Fig. 8B). In this case, the theoretical maximum respiration rate of the cell is limited by diffusion. When both diffusion limitation and the enzyme K_m (21 nmol liter^{-1}) are taken into account, the apparent K_m value obtained from the curve is much higher than the enzymatic K_m value (5 nmol liter^{-1}). We observed an even higher apparent K_m value of 43 nmol liter^{-1} under nonlimited conditions, indicating that our geometric assumptions were oversimplified. Under these conditions, R_c values are close to J_{max} values at the lowest O_2 concentrations. (iii) When the environment is low in electron donors, the decrease in cell size and low respiration rates enabled the actual respiration rate to get very close to the theoretical non-diffusion-limited respiration rate (Fig. 8C). The apparent K_m value (7 nmol liter^{-1}) was similar to the values measured experimentally and approached the enzymatic K_m value, and V_{max} was thus approached at very low O_2 concentrations. It is thus an advantage for the bacterium to decrease its cell size under conditions of limitation of O_2 (or any other type of element) (32). Marine bacteria thus decrease their cell volume when nutrients are present at low concentrations (33, 34).

K_m values measured by different methods were summarized in a previous study (23). Until 1994, studies showed that the K_m values measured by an O_2 electrode are higher than the K_m values estimated from the deoxygenation kinetics of myoglobin or leghemoglobin. That might probably indicate that the latter method has a resolution higher than that achieved with standard Clark-type O_2 electrodes. Furthermore, the apparent K_m values for *E. coli* in exponential phase determined with a sensitive O_2 electrode were found to be 1.80 μmol liter^{-1} (20) and 0.19 μmol liter^{-1} (18) in two studies. This 1-order-of-magnitude difference in these two apparent K_m values suggests that the sensitivity of the electrode affects the determination of the apparent K_m value and that the estimates are nonrealistic. The apparent K_m values determined even by our extremely sensitive O_2 microsensors with a fast response were at least twice the values estimated by optodes for the four species investigated in this experiment (data not shown). The technique relying on the spectrophotometric differences between the oxygenated and deoxygenated state of myoglobin or leghemoglobin was applied more often than the technique with O_2 electrodes after the 1980s to determine K_m values for different types of terminal oxidases or whole cells of *E. coli* (17, 35), pathogens (36), and soil bacteria (23, 37). Previously reported K_m values obtained by this technique were also in the nanomolar range. However, the reported K_m values determined by the use of leghemoglobin and myoglobin can have a 1-order-of-magnitude difference in the same study (35, 36). Furthermore, it has been observed that the apparent K_m values measured with intact cells (*Azotobacter vinelandii*) which contain a cytochrome *bd*-type oxidase (a typical high-affinity terminal oxidase) are 4-fold higher than those measured in membranes (23). High apparent K_m values indicate a diffusion limitation of the O_2 supply. In addition, a previous study showed that the level of expression of the gene encoding the low-affinity terminal oxidase is repressed over 140-fold under anaerobic conditions in *E. coli* but is still detectable (29). Thus, some low-affinity terminal oxidases may still be functioning even in environments with extremely low O_2 concentration, which could contribute to relatively high apparent K_m values. The values estimated in our study even surpass the bottom of the range of apparent K_m values for intact cells reported previously, and we thus assume that the set of techniques used is more sensitive than previously used methods.

In comparison with previous studies related to respiration kinetics, the advantages of this study are as follows. (i) The setup used in this study enables the continuous recording of the O_2 concentration. Thus, it is able to resolve temporal change in kinetics. Previous studies focused on the respiration of bacteria and the apparent K_m value of the bacteria during some kind of supposed steady state. It has been recorded that apparent K_m values for *E. coli* in early exponential phase and stationary phase have almost a 1-order-of-magnitude difference (1.80 and 0.27 μmol liter^{-1}, respectively) in the same study (20). We know, however, that the apparent K_m value of bacteria must be related to the range of O_2 concentrations during the incubation, as a certain transition concentration triggers the expression of high-affinity terminal oxidases (38). However, the change of kinetics for the same types of cells over time is apparently neglected. The myoglobin- or leghemoglobin-based method resolves only the apparent K_m values for one state of the cells rather than a temporal change. This study reveals that the apparent K_m values decrease over time under conditions with low O_2 concentrations and a limited electron donor supply. (ii) The system is completely sealed by glass, except for the pressure compensation tube, which is used for the injection of bacteria and water, and this creates a system that is more isolated from the environment than previous setups. The myoglobin- or leghemoglobin-based method requires a stopper with a fine hole to seal the cuvette (23). Ambient O_2 can easily pass through the hole and the gap between the stopper and the cuvette to contaminate the system. Furthermore, our setup can be applied to all types of aquatic media.

The optical trace O_2 sensor allows the measurement of respiration rates under conditions with low O_2 levels with a high sensitivity and an extremely low detection limit. The apparent K_m values estimated from this study are lower than those previously reported in studies of isolated marine bacteria in culture (39) and seawater (22). The conditions of our incubations with energy limitation are closer to *in situ* ocean conditions than traditional incubations in rich media. As a consequence of starvation, the reduced respiration rate per cell and the reduced cell size decreased the diffusion limitation and resulted in lower apparent K_m values, illustrating that even individual fast-respiring bacteria are diffusion limited at very low O_2 concentrations. The same holds true for all other substances present in low concentrations.

ACKNOWLEDGMENTS

We gratefully acknowledge Preben G. Sørensen and Lars B. Pedersen for their technical assistance. We thank glass blower J. C. Kondrup at Aarhus University for providing the incubation reactors. We acknowledge Yao Chen for helping with illustrations. The FACS Core facility at Aarhus University provided access to flow cytometer equipment.

This study was supported by the European Research Council (grant no. 2672333).

FUNDING INFORMATION

EC | European Research Council (ERC) provided funding to Xianzhe Gong, Emilio Garcia-Robledo, and Niels Peter Revsbech under grant number 2672333.

The funders had no role in study design, data collection and interpretation, or the decision to submit the work for publication.

REFERENCES

1. **Canfield DE, Kristensen E, Thamdrup B.** 2005. Aquatic geomicrobiology. Advances in marine biology, vol 48. Elsevier Academic Press, San Diego, CA.
2. **Kühl M.** 2005. Optical microsensors for analysis of microbial communities. Methods Enzymol **397:**166–199. http://dx.doi.org/10.1016/S0076-6879(05)97010-9.
3. **Nielsen LP, Christensen PB, Revsbech NP, Sørensen J.** 1990. Denitrification and oxygen respiration in biofilms studied with a microsensor for nitrous oxide and oxygen. Microb Ecol **19:**63–72. http://dx.doi.org/10.1007/BF02015054.
4. **Allee WC, Oesting R.** 1934. A critical examination of Winkler's method for determining dissolved oxygen in respiration studies with aquatic animals. Physiol Zool **7:**509–541.
5. **Williams PJL.** 1984. A review of measurements of respiration rates of marine plankton populations, p 357–389. *In* Hobbie JE, Williams PJL (ed), Heterotrophic activity in the sea. Springer USA, Boston, MA.
6. **Martínez-García S, Karl DM.** 2015. Microbial respiration in the euphotic zone at Station ALOHA. Limnol Oceanogr **60:**1039–1050. http://dx.doi.org/10.1002/lno.10072.
7. **Kirchman DL.** 1997. Carbon cycle: microbial breathing lessons. Nature **385:**121–122. http://dx.doi.org/10.1038/385121a0.
8. **Falkowski PG, Algeo T, Codispoti L, Deutsch C, Emerson S, Hales B, Huey RB, Jenkins WJ, Kump LR, Levin LA, Lyons TW, Nelson NB, Schofield OS, Summons R, Talley LD, Thomas E, Whitney F, Pilcher CB.** 2011. Ocean deoxygenation: past, present, and future. Eos Trans Am Geophys Union **92:**409. http://dx.doi.org/10.1029/2011EO460001.
9. **Tiano L, Garcia-Robledo E, Dalsgaard T, Devol A, Ward BB, Ulloa O, Canfield DE, Revsbech NP.** 2014. Oxygen distribution and aerobic respiration in the north and south eastern tropical Pacific oxygen minimum zones. Deep Sea Res Part I Oceanogr Res Pap **94:**173–183. http://dx.doi.org/10.1016/j.dsr.2014.10.001.
10. **Wikner J, Panigrahi S, Nydahl A, Lundberg E, Bamstedt U, Tengberg A.** 2013. Precise continuous measurements of pelagic respiration in coastal waters with oxygen optodes. Limnol Oceanogr Methods **11:**1–15. http://dx.doi.org/10.4319/lom.2013.11.1.
11. **Kalvelage T, Lavik G, Jensen MM, Revsbech NP, Löscher C, Schunck H, Desai DK, Hauss H, Kiko R, Holtappels M, LaRoche J, Schmitz RA, Graco MI, Kuypers MMM.** 2015. Aerobic microbial respiration in oceanic oxygen minimum zones. PLoS One **10:**e0133526. http://dx.doi.org/10.1371/journal.pone.0133526.
12. **Poole RK.** 1983. Bacterial cytochrome oxidases: a structurally and functionally diverse group of electron-transfer protein. Biochim Biophys Acta **726:**205–243. http://dx.doi.org/10.1016/0304-4173(83)90006-X.
13. **Hemp J, Robinson DE, Ganesan KB, Martinez TJ, Kelleher NL, Gennis RB.** 2006. Evolutionary migration of a post-translationally modified active-site residue in the proton-pumping heme-copper oxygen reductases. Biochemistry **45:**15405–15410. http://dx.doi.org/10.1021/bi062026u.
14. **Calhoun MW, Thomas JW, Gennis RB.** 1994. The cytochrome oxidase superfamily of redox-driven proton pumps. Trends Biochem Sci **19:**325–330. http://dx.doi.org/10.1016/0968-0004(94)90071-X.
15. **Pitcher RS, Watmough NJ.** 2004. The bacterial cytochrome cbb_3 oxidases. Biochim Biophys Acta **1655:**388–399. http://dx.doi.org/10.1016/j.bbabio.2003.09.017.
16. **Brändén G, Gennis RB, Brzezinski P.** 2006. Transmembrane proton translocation by cytochrome *c* oxidase. Biochim Biophys Acta **1757:**1052–1063. http://dx.doi.org/10.1016/j.bbabio.2006.05.020.
17. **D'Mello R, Hill S, Poole RK.** 1996. The cytochrome *bd* quinol oxidase in *Escherichia coli* has an extremely high oxygen affinity and two oxygen-binding haems: implications for regulation of activity *in vivo* by oxygen inhibition. Microbiology **142:**755–763. http://dx.doi.org/10.1099/00221287-142-4-755.
18. **Rice CW, Hempfling WP.** 1978. Oxygen-limited continuous culture and respiratory energy conservation in *Escherichia coli*. J Bacteriol **134:**115–124.
19. **Smith A, Hill S, Anthony C.** 1990. The purification, characterization and role of the *d*-type cytochrome oxidase of *Klebsiella pneumoniae* during nitrogen fixation. J Gen Microbiol **136:**171–180. http://dx.doi.org/10.1099/00221287-136-1-171.
20. **Kita K, Konishi K, Anraku Y.** 1984. Terminal oxidases of *Escherichia coli* aerobic respiratory chain. II. Purification and properties of cytochrome b_{558}-*d* complex from cells grown with limited oxygen and evidence of branched electron-carrying systems. J Biol Chem **259:**3375–3381.
21. **Appleby CA, Bergersen FJ.** 1980. Preparation and experimental use of leghaemoglobin, p 315–335. *In* Bergersen FJ (ed), Methods for evaluating biological nitrogen fixation. John Wiley & Sons, Chichester, United Kingdom.
22. **Tiano L, Garcia-Robledo E, Revsbech NP.** 2014. A new highly sensitive method to assess respiration rates and kinetics of natural planktonic communities by use of the switchable trace oxygen sensor and reduced oxygen concentrations. PLoS One **9:**e105399. http://dx.doi.org/10.1371/journal.pone.0105399.
23. **D'Mello R, Hill S, Poole RK.** 1994. Determination of the oxygen affinities of terminal oxidases in *Azotobacter vinelandii* using the deoxygenation of oxyleghaemoglobin and oxymyoglobin: cytochrome *bd* is a low-affinity oxidase. Microbiology **140:**1395–1402. http://dx.doi.org/10.1099/00221287-140-6-1395.
24. **Lehner P, Larndorfer C, Garcia-Robledo E, Larsen M, Borisov SM, Revsbech N-P, Glud RN, Canfield DE, Klimant I.** 2015. Lumos—a sensitive and reliable optode system for measuring dissolved oxygen in the nanomolar range. PLoS One **10:**e0128125. http://dx.doi.org/10.1371/journal.pone.0128125.
25. **Borisov SM, Lehner P, Klimant I.** 2011. Novel optical trace oxygen sensors based on platinum(II) and palladium(II) complexes with 5,10,15,20-*meso*-tetrakis-(2,3,4,5,6-pentafluorphenyl)-porphyrin covalently immobilized on silica-gel particles. Anal Chim Acta **690:**108–115. http://dx.doi.org/10.1016/j.aca.2011.01.057.
26. **Hansen H, Koroleff F.** 1999. Determination of nutrients, p 159–224. *In* Grasshoff K, Kremling K, Ehrhardt M (ed), Methods of seawater analysis. Wiley-VCH, Weinheim, Germany.
27. **Holert J, Hahnke S, Cypionka H.** 2011. Influence of light and anoxia on chemiosmotic energy conservation in *Dinoroseobacter shibae*. Environ Microbiol Rep **3:**136–141. http://dx.doi.org/10.1111/j.1758-2229.2010.00199.x.
28. **Laass S, Kleist S, Bill N, Drüppel K, Kossmehl S, Wöhlbrand L, Rabus R, Klein J, Rohde M, Bartsch A, Wittmann C, Schmidt-Hohagen K, Tielen P, Jahn D, Schomburg D.** 2014. Gene regulatory and metabolic adaptation processes of *Dinoroseobacter shibae* DFL12^T during oxygen depletion. J Biol Chem **289:**13219–13231. http://dx.doi.org/10.1074/jbc.M113.545004.
29. **Cotter PA, Chepuri V, Gennis RB, Gunsalus RP.** 1990. Cytochrome *o* (*cyoABCDE*) and *d* (*cydAB*) oxidase gene expression in *Escherichia coli* is regulated by oxygen, pH, and the *fnr* gene product. J Bacteriol **172:**6333–6338.
30. **Jørgensen BB.** 2001. Life in the diffusive boundary layer, p 348–373. *In* Boudreau BP, Barker JB (ed), The benthic boundary layer. Oxford University Press, New York, NY.
31. **Yoon J-H, Yeo S-H, Kim I-G, Oh T-K.** 2004. *Marinobacter flavimaris* sp. nov. and *Marinobacter daepoensis* sp. nov., slightly halophilic organisms isolated from sea water of the Yellow Sea in Korea. Int J Syst Evol Microbiol **54:**1799–1803. http://dx.doi.org/10.1099/ijs.0.63151-0.
32. **Koch AL.** 1971. The adaptive responses of *Escherichia coli* to a feast and famine existence. Adv Microb Physiol **6:**147–217. http://dx.doi.org/10.1016/S0065-2911(08)60069-7.
33. **Kjelleberg S, Humphrey BA, Marshall KC.** 1982. Effect of interfaces on small, starved marine bacteria. Appl Environ Microbiol **43:**1166–1172.
34. **Kjelleberg S, Hermansson M.** 1984. Starvation-induced effects on bacterial surface characteristics. Appl Environ Microbiol **48:**497–503.
35. **D'Mello R, Hill S, Poole R.** 1995. The oxygen affinity of cytochrome *bo′* in *Escherichia coli* determined by the deoxygenation of oxyleghemoglobin and oxymyoglobin: K_m values for oxygen are in the submicromolar range. J Bacteriol **177:**867–870.
36. **Wainwright LM, Elvers KT, Park SF, Poole RK.** 2005. A truncated haemoglobin implicated in oxygen metabolism by the microaerophilic food-borne pathogen *Campylobacter jejuni*. Microbiology **151:**4079–4091. http://dx.doi.org/10.1099/mic.0.28266-0.

37. **Contreras ML, Escamilla JE, Del Arenal IP, Davila JR, D'Mello R, Poole RK.** 1999. An unusual cytochrome *o′*-type cytochrome *c* oxidase in a *Bacillus cereus* cytochrome a_3 mutant has a very high affinity for oxygen. Microbiology **145:**1563–1573. http://dx.doi.org/10.1099/13500872-145-7-1563.
38. **Bergersen FJ, Turner GL.** 1980. Properties of terminal oxidase systems of bacteroids from root nodules of soybean and cowpea and of N_2-fixing bacteria grown in continuous culture. Microbiology **118:**235–252. http://dx.doi.org/10.1099/00221287-118-1-235.
39. **Devol AH.** 1978. Bacterial oxygen uptake kinetics as related to biological processes in oxygen deficient zones of the oceans. Deep Sea Res **25:**137–146. http://dx.doi.org/10.1016/0146-6291(78)90001-2.